Construction and Building Materials 300 (2021) 124013

Contents lists available at ScienceDirect

Construction and Building Materials

journal homepage: www.elsevier.com/locate/conbuildmat

# Novel invisible markers for monitoring cracks on masonry structures

İhsan E. Bal [a,*], Dimitris Dais [a,b], Eleni Smyrou [a], Vasilis Sarhosis [b,c]

[a] Research Centre for Built Environment, Hanze University of Applied Sciences, Groningen, the Netherlands
[b] School of Civil Engineering, University of Leeds, Leeds LS2 9JT, UK
[c] ISCARSAH-UK, Analysis and Restoration of Structures of Architectural Heritage, UK

## HIGHLIGHTS

- Novel near-infrared (NIR) markers were developed for crack monitoring.
- Painted markers perform better than the tape markers both in terms of accuracy and precision.
- Precision and accuracy of 0.05 mm has been achieved.
- Markers are almost invisible and thus aesthetically pleasing for historical structures.
- The method can be used by non-technical people; citizen involvement is encouraged.

## ARTICLE INFO

*Article history:*
Received 22 January 2021
Received in revised form 14 June 2021
Accepted 15 June 2021

*Keywords:*
Near-infrared markers
Crack monitoring
Image processing
Non-destructive assessment

## ABSTRACT

This paper presents a proof of concept for monitoring masonry structures using two different types of markers which are not easily noticeable by human eye but exhibit high reflection when subjected to NIR (near-infrared) wavelength of light. The first type is a retroreflective marker covered by a special tape that is opaque in visible light but translucent in NIR, while the second marker is a paint produced from infrared reflective pigments. The reflection of these markers is captured by a special camera-flash combination and processed using image processing algorithms. A series of experiments were conducted to verify their potential to monitor crack development. It is shown that the difference between the actual crack width and the measured was satisfactorily small. Besides that, the painted markers perform better than the tape markers both in terms of accuracy and precision, while their accuracy could be in the range of 0.05 mm which verifies its potential to be used for measuring cracks in masonry walls or plastered and painted masonry surfaces. The proposed method can be particularly useful for heritage structures, and especially for acute problems like foundation settlement. Another advantage of the method is that it has been designed to be used by non-technical people, so that citizen involvement is also possible in collecting data from the field.



## 1. Introduction

A significant amount of the building stock (houses, transportation infrastructure, historically important buildings etc.) in the world consists of masonry of various types. Monitoring several of these structures in order to ensure that they do meet the modern standards and are safe for use becomes of vital importance. Continuous monitoring can extend the life span of these structures by allowing the decision makers to take necessary measures for repair and strengthening.

Continuous monitoring of masonry structures can be done in various forms. In particular, structural health monitoring (SHM) with an accelerometer sensor network, combined with other sensors for collecting continuous vibrational deformation and environmental data from a structure, has been used and reported in the literature [1–4]. Non-destructive testing (NDT) techniques are common too [5]. Acoustic emission, an example of NDT approach, can also be applied for the identification and localization of damage on masonry structures [6,7]. Alternatively, one-time monitoring can be conducted by using vision-based methods, such as DIC (Digital Image Correlation), photogrammetry or laser scanning [8–15]. The described methods, i.e. SHM, (non-destructive) testing and vision-based techniques, provide crucial information on the damage identification and quantification. Nevertheless, these techniques cannot be rapidly employed when screening of numerous structures is required after a damaging event. As far as earthquakes are concerned, it is simply not feasible to perform assessment on

* Corresponding author.
*E-mail address:* i.e.bal@pl.hanze.nl (İ.E. Bal).

https://doi.org/10.1016/j.conbuildmat.2021.124013
0950-0618/

every structure to quantify residual deformations and damages. Furthermore, the vast majority of structures does not have a monitoring system installed. Vision-based techniques, on the other hand, usually require expensive equipment and skilled personnel to operate them. In particular, the DIC approaches entail a cumbersome procedure (surface preparation, lighting conditions, DIC algorithms etc.) and thus are mainly limited to laboratory conditions [16,17]. Due to these drawbacks, assessment of structures heavily relies on manual damage inspection based on data mostly obtained visually and manually. Nevertheless, this practice is rather laborious, slow, subjective and expensive when accounting for the man-hours required to be invested in the field and at the office to process the collected data. Moreover, manual inspection can raise safety concerns, since there are parts of structures with access restrictions and difficult to reach.

In order to assist the inspection process, novel artificial intelligence (AI) methods for vision-based assessment and monitoring of civil infrastructures are gaining ground nowadays [18]. In particular, extensive research has been devoted to detect defects such as cracks by using photographs from concrete or asphalt surfaces without any prior surface preparation [19–22]. Innovative ideas, such as following the masonry deformations via a grid of dot markers and connecting these measurements with numerical analyses as reported by Stockdale et al. [23–25], can provide new insights in otherwise challenging masonry nonlinear behavior. More recently, Dais et al. [26] introduced an approach where detection of cracks can be done accurately on pixel level on masonry surfaces. Rezaie et al. [27] implemented AI-assisted crack segmentation on laboratory images taken for DIC. These cutting-edge technologies have the potential to facilitate significantly the assessment of structures by detecting cracks. Maintenance of historical structures, particularly of those facing problems such as foundation settlement, is one of the main areas where continuous structural monitoring is needed. Bal et al. [28] introduced a tailor-made structural health monitoring scheme for a historical masonry structure subjected to induced-seismicity events. In this study the importance of crack monitoring for a reliable damage assessment was showcased. Carrillo et al. [29] and Farhidzadeh et al. [30] emphasized that the characteristics of cracks as obtained from the inspection process, e.g. length, width, pattern and distribution, are important indicators of structural damage, while a quantification of damage based on residual cracks was performed numerically by Sarhosis et al. [31]. While the significance of monitoring of the crack characteristics was established [28–31], it is highlighted that the methods for automatic crack detection from photographs lack the ability to detect the crack width accurately [26,32,33], especially in the sub-millimeter region, a parameter that can provide crucial information on the severity and the progression of the damage. Without surface preparation, the information reflected in a photograph highly depends on the photographic conditions, especially on the amount and angle of the light, while the accurate width measurement of thin edges, such as cracks, is hard to be achieved. Various methods were developed in the past to overcome this problem, relying on monitoring certain type of markers around the cracks instead of monitoring the crack itself [32-36]. It is stressed that these markers are highly visible and especially for the cases of monumental structures, where strict regulations apply, even simple interventions, such as placing crack-rulers, are not permitted by the conservation authorities. AI techniques for automatic crack segmentation and measurement have been presented [20,33] for rather homogeneous surfaces, such as asphalt and concrete, but their applicability for crack width measurement at complex surfaces, that is masonry, might be limited.

The crack detection by using image processing methods arises as a suitable NDT solution based on the discussion above, provided that the markers and their reflection of light are not easily visible. A novel NIR marker methodology is proposed in this paper. Three main challenges are attempted to be addressed by the crack monitoring with the novel NIR markers: providing continuous and low-cost monitoring without needing high technical skills, focusing on cracks and progression of damage, and being discreet enough to be appropriate for applications on real structures. The proposed method here shifts the marker reflection and its contrast with the background into the invisible wavelength of light (i.e. to the near-infrared) so that the markers are not easily distinguishable. The method is thus particularly suitable for monitoring historical buildings. For instance, by using the monitoring data from this method, a back analysis could be conducted by using limit analysis approaches [37–39] for damaged historical masonry structures. The method allows time-stamped continuous monitoring since the digital photograph files automatically contain additional information on the location of the object, camera exposure and intrinsic parameters, as well as the date and time stamp. The method is also suitable for automatized monitoring of a large inventory of structures where the data can be collected by non-technical people or citizens and uploaded on a web server for processing.

## 2. NIR markers and crack measurement

Square markers are used in this study. The square shape of the marker is more in line with the masonry texture, making the markers even more invisible. Furthermore, a group of 4 markers is used for forming a gauge on each side of a crack. The 4-marker configuration decreases the errors and renders the marker setup more durable in case of loss of a marker.

As shown in Fig. 1(a), two groups of markers, each group consisting of 4 identical markers, are designed to be placed on both sides of a crack. Unlike conventional sensors, such as LVDTs or potentiometers, which only measure along their axis, the approach proposed herein can detect deformations along any direction in the plane of the markers. Image processing algorithms can filter out the shining markers by creating a binary (i.e. black & white) photo from an image like in Fig. 1(d), a process explained later in the paper. In this process, the centroid of each marker is calculated pixel-wise, and then the centroid of each marker group is calculated by averaging the coordinates of each group of markers (i.e. left and right quadruple). The vertical and the horizontal distance between the two centroids of markers quadruples is then used to monitor the crack width in between.

The procedure described here is designed so that a non-technical person can also place the markers and take the photographs. This will allow citizen involvement, a procedure that can tremendously increase the amount of data while decreasing the costs. In order to replicate this in the tests presented here, three issues have been taken care of:

i) Materials commercially available and easily accessible in the market are used (including the camera and the flashlight)
ii) The photos are taken by holding the camera always in hand, without a tripod
iii) Instead of large and fixed flash sources like those commonly used in laboratory applications, a simple hot-shoe NIR flash attached on the camera as the main light source.

Two types of markers were tested: i) tape markers, and ii) reflective paint markers (Table 1). The tape markers are intended for use directly on clay brick surfaces without any surface preparation. The reflective paint markers are for brick masonry, plastered or painted surfaces. Details of these markers are given in Sections 2.2 and 2.3. Both types of markers, although they do not match perfectly with the background color, exhibit color tones very close

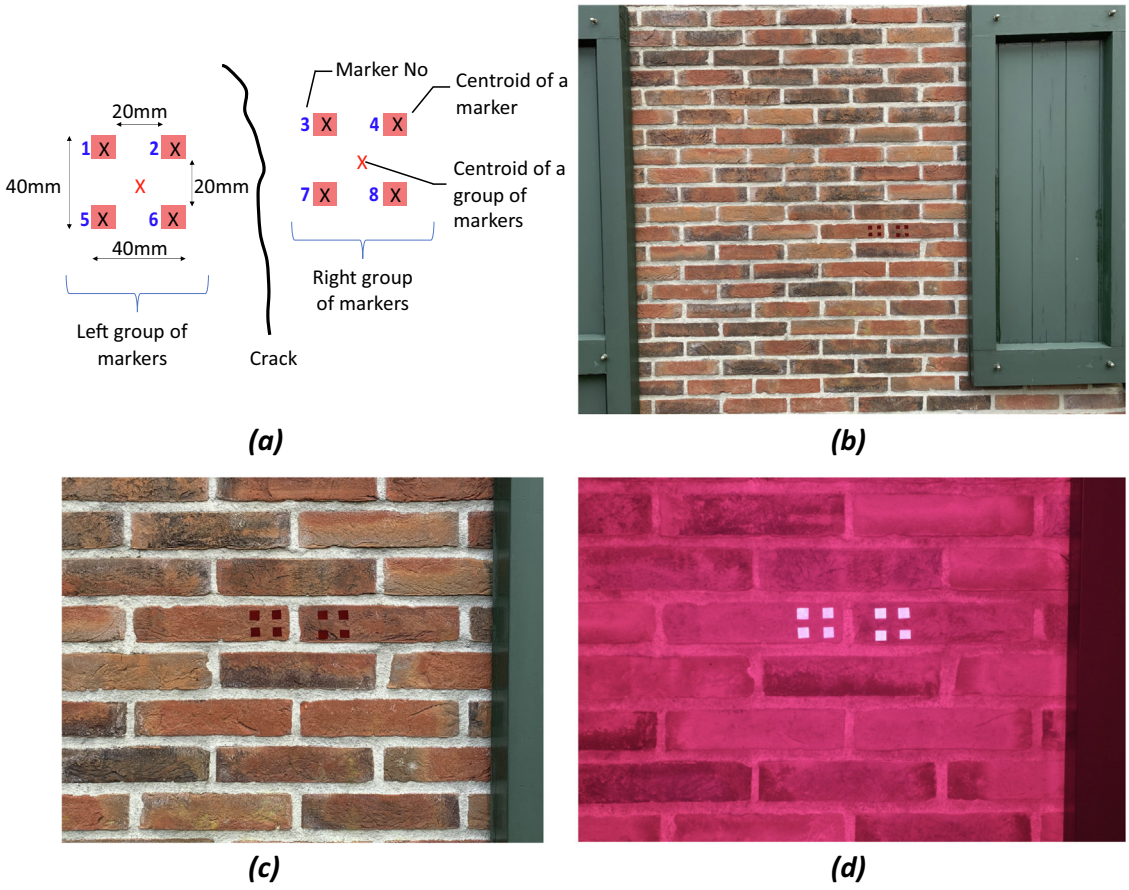


**Fig. 1.** (a) Schematic view of the proposed marker setup and the marker numbering, (b) NIR markers on the outer wall of a real masonry house, (c) close-up view of the NIR markers in the visible light, and (d) close-up photo of the markers captured with the special NIR camera.

to the background making it hard to be distinguished by human eye.

### 2.1. NIR camera and hot-shoe flashlight

The NIR images used in this study were taken by a commercially available DSLR (digital single-lens reflect) type camera and a compatible hot-shoe flashlight. The camera and the flashlight were modified to be able to work only in the NIR region of light. A commercially available 24MP DSLR consumer camera was modified by using a longpass filter (Hoya RM90) that transmits 50% of light at 920 nm. Longpass filter means that the filter will allow only above a certain wavelength of light to pass. Besides that, the flash attached on the camera has a longpass filter that is rated as 715 nm (i.e. 50% of light passes at 715 nm wavelength). The relation of the sensitivity areas of the camera and the flash in respect to the visible light can be seen in Fig. 2.

The camera intrinsic parameters and the photograph exposure play a major role in the accuracy and precision of the procedure. The key parameters that were evaluated are i) focal length, ii) shutter speed, iii) brightness (ISO), iv) aperture (F), and v) flash intensity. The focal length is set to 55 mm and kept constant in all photographs; this is because in this setting the distortion of the planar view due to the lens is minimized. The shutter speed, which defines the duration the camera lens stays open, is also set to a constant value as 125 (i.e. 1/125th of a second) which allows sufficient time so that enough light falls on the camera sensor but short enough not to lead to blurry edges when a tripod is not used. The rest of the parameters are set according to the marker type and the camera distance.

The NIR tape markers are used directly on clay brick surfaces while infrared reflective paint is used on painted surfaces. When tape markers are used on a clay brick surface, and because the clay is also an infrared reflective material, brick surface shines more than a normal surface. In order to keep the contrast between the clay brick background and the tape markers, F18 and ISO400 settings are used in all photographs in order to achieve smaller brightness for the background.

The painted surfaces absorb more NIR light than the clay brick surfaces and appear relatively dark in the photos while the infrared reflective paint is shining. This is also one of the main reasons why infrared reflective paints are used widely in automotive and construction industry. The infrared part of the sunlight is reflected back thanks to the infrared reflective pigments, which are also called "cool pigments", keeping the indoors cooler in hot summer days. This reflection keeps the surfaces painted with this special pigment cooler than the surfaces painted with a normal paint. In the case of the reflective paint markers, more light needs to be emitted on the surface to create an acceptable level of contrast between the normal painted background and the reflective markers. This is the reason why F10 ISO1000 is used for the photos for the NIR reflective paint markers. The difference between the two settings (i.e. F18/ISO400 for the tape markers versus F10/ISO1000 for the paint markers) is evident when Fig. 4 is compared to Fig. 3. The binary photos are mostly dark in Fig. 3 (tape markers) while the background is white in Fig. 4 (paint markers).

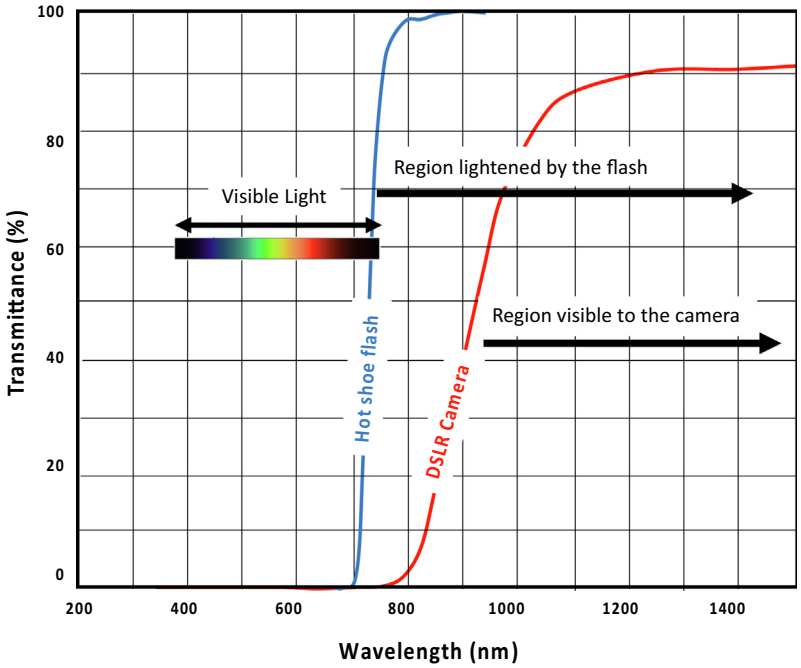


**Fig. 2.** Comparison of the wavelength of the visible light, the visible region for the modified DSLR camera and the modified hot-shoe flash used in this study.

The flashlight used in this application is able to produce light in varying intensities. The intensity of the flash can automatically be detected by the flash depending on the distance from the object. However, this function does not work well in the NIR flash and camera combination. Instead, the flash intensity was set manually, by trying several options and finding manually a range of acceptable flash intensities for each camera distance. It is further discussed later that the flash intensity plays a major role in the accuracy and precision of the method, since it is the prime source of light produced in the NIR region. It is shown below that if the flash is either too strong or too weak, the accuracy deteriorates significantly. The flash intensity can be set from 1.0 (100%) to 1/2 (50%), 1/4 (25%) and so on. There are also three steps between these flash intensities, i.e between 100% and 50% (Table 2).

### 2.2. NIR tape markers

The idea behind the NIR tape markers is simple as the main reflective material is a *retro*-reflective tape, similar to those used in laboratory applications of structural testing [17]. The *retro*-reflection allows the flashlight emitted by the reflector to always return to the camera, a property that minimizes the errors caused by varying camera angles. These are white stickers that are visible in daylight and shine in dark when subjected to any source of light. They are thus not directly usable for applications in real structures as they would create a disturbing view both in day and night. To avoid that, the retroreflective material is covered with a special tape used in photography, made of a derivation of plastic (PV1 – polyvinyl). This material is opaque in the visible light and becomes translucent in the NIR region. The first layer of retroreflective material is covered with a sticky layer beneath for application on the wall surfaces. These 3-layer markers are then cut 10mmx10mm dimensions and placed in the configuration as shown in Fig. 1(a).

The PV1 tapes are available in the market exclusively in ruby color because of their use in photography. If these markers to be produced for other purposes, then varying colors, to better match the background brickwork texture, can be obtained. The tape markers would become even less visible in this case.

Another issue with the application of these markers is making perfect shapes. The markers used in this paper were manually produced and applied on brick samples. This yielded into a non-perfect configuration of marker arrangement and also imperfect marker dimensions. If these parameters be industrialized, further accuracy and precision can be achieved.

Finally, the tape markers were applied on the brick surfaces with simple glued industrial paper, which is not necessarily durable enough for outdoor applications. Furthermore, the markers were used for short term measurements without actually being tested in terms of UV resistance. Application details of this sort need to be addressed before applying the technology on actual structures.

The actual view of the test setup from varying distances, as well as the NIR photos and the processed binary photos from the specimens with the tape markers can be found in Fig. 3.

### 2.3. NIR reflective paint markers

NIR reflective paint markers are applied on already painted surfaces (Fig. 4) although they can also be directly used on brick masonry. There are various colors available in the market. For the purposes of this study dark brown color is used for the paint markers. The background was painted with a similar color of paint suitable for outdoor applications. A template was cut from glued paper, placed on the painted brick surfaces, and then the infrared reflective paint was applied on the brick surface with a home-type paint spray to make sure a homogenous spread of paint material within the markers. A similar configuration to that of the tape markers is kept also in the paint markers.

Infrared reflective pigments are available in the market as dust. They need to be mixed with a correct type of binder (a liquid epoxy-based mixture) to become a paint and be able to adhere on the surface of application. The NIR light reflection ability of pigments depends on the color since the color is the outcome of the material the pigments are produced from. Although a variety of

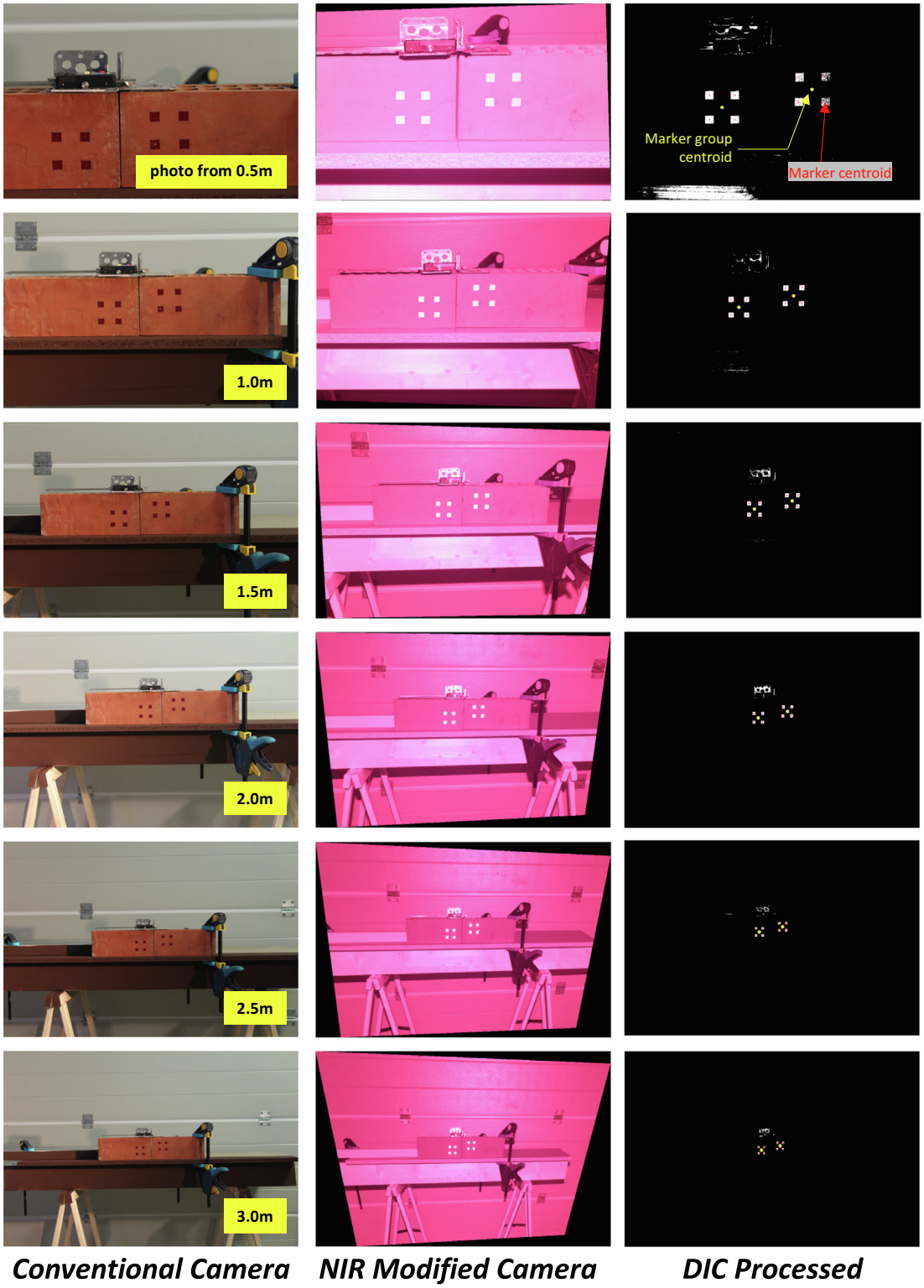


**Fig. 3.** Photos taken by a conventional camera (left), photos taken by the near-infrared modified DSLR camera and perspective correction is applied (middle), and binary (black & white) photos created by the image processing procedure from the perspective corrected photos (right) of the NIR tape markers.

colors is available commercially, these pigments are intended for industrial use and sold only in large quantities. It was rather difficult to get small sample quantities for the purposes of this study, so only one color (dark brown) is tested here. However, various other colors can also be used in the exact same configuration, better matching the painted color of the background.

The main advantage of the paint markers is that the application is very simple and the impact on the structure is almost none. Because the paint is only a very thin layer, it is also more difficult to be distinguished as compared to the tape markers, which need special attention on how to stick to the brick surface and how to provide UV protection. Adherence to the surface and the UV

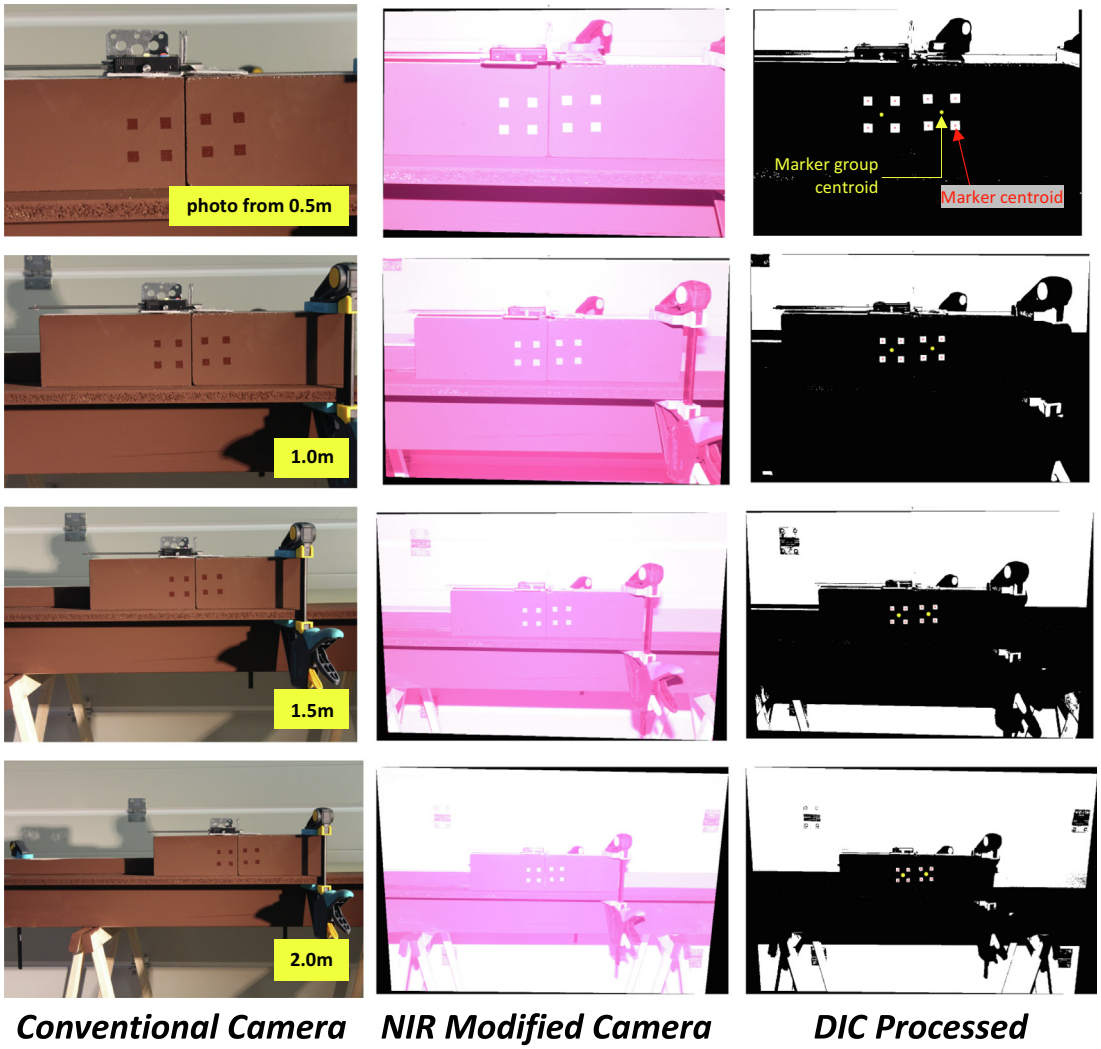


**Fig. 4.** Photos taken by a conventional camera (left), photos taken by the near-infrared modified DSLR camera and perspective correction is applied (middle), and binary (black & white) photos created by the image processing procedure from the perspective corrected photos (right) of the NIR paint markers.

protection problems are automatically solved in the NIR paint markers.

The NIR paint markers were also tested directly on clay brick surfaces. However, as mentioned before, clay is also an infrared reflective material, thus the reflection from the paint markers does not create a large enough contrast with the background, an issue that needs further investigation.

### 2.4. Test setup

Both types of markers, i.e. tape and reflective paint markers, were applied on brick surfaces by using the configuration presented in Fig. 1(a). Properties of the two marker types are listed in Table 1. Photos were then taken at camera distances of 0.5, 1.0, 1.5, 2.0, 2.5 and 3.0 m. In each distance, two or three different flash intensities were used as shown in Table 2.

The test setup consists of two bricks as shown in Fig. 5. One of the bricks is fixed while the other is slightly moved to the sideway in each set of photos. The two marker quadruples are separated from each other in this way, simulating a crack in a real-life example. The movement of one brick in respect to the other was measured with a digital caliper with mm/100 precision. The moving brick was moved along a guide in order to keep the movement within the marker plain. A set of photographs were taken first without any separation between the bricks, where the caliper was set to zero. Separations of 0.23, 0.56, 1.20, 1.80, 2.40, 3.53 and 5.00 mm were applied on the setup of the tape markers while 0.25, 0.53, 1.18, 1.91, 2.59, 3.70 and 5.04 mm separations were imposed in the case of paint markers.

**Table 1**
Properties of the tape and paint markers.

| Marker Property | Tape Marker | Paint Marker |
|---|---|---|
| Material | From brick surface to outwards composed of 3 layers as: adhesive tape, retroreflective tape, NIR translucent tape | NIR reflective dust pigments mixed with epoxy-based binding agent |
| Configuration | 2 marker groups on each side of the crack, each group with 4 markers at the corners of a square (see Fig. 1a) | |
| Marker Dimensions | 10 mm × 10 mm each marker, 40x40mm bounding box for each marker group | |
| Application to the surface | Stuck with an adhesive tape | Painted with a spray paint gun, over a custom-made template |
| Surfaces suitable | Naked brick, plastered or painted surfaces | |
| UV protection | No | Yes |

**Table 2**
Camera distances and flash intensities used in the tests.

| Camera Distance (m) | Flash Intensity Notation | Flash Intensity (%) |
|---|---|---|
| 3.0 | 1/1 | 100 |
| 2.5 | 1/1 | 100 |
| 2.0 | 1/1 | 10,085 |
| | 1/1–0.3 | |
| 1.5 | 1/1–0.3 | 856,550 |
| | 1/1–0.7 | |
| | 1/2 | |
| 1.0 | 1/2 | 50 |
| | 1/2–0.3 | 42.5 |
| | 1/2 – 0.7 | 32.5 |
| 0.5 | 1/4 | 25 |
| | 1/4 – 0.3 | 21.25 |

Distances to tha markers were marked on the floor and a photo was taken by hand (i.e. without the use of tripod) from each distance, standing on these marks on the floor, following the flash intensity ranges shown in Table 2. As shown in Fig. 3 and in Fig. 4 (middle column), the photos were taken from arbitrary horizontal and vertical angles as expected result of a manual process of photo taking.

### 2.5. Perspective correction

Crack monitoring entails revisiting a location multiple times to extract measurements. Given the fact that the camera is kept in hand and not fixed to a constant point, corrections need to be accounted for the camera pose of each measurement (see Fig. 6 for an example). In other words, a so-called homography transformation (a 3×3 matrix) is performed to map the points in one image to the corresponding points in a reference image [40–42]. The planar homography matrix relates the transformation between two planes (up to a scale factor) with the following relationship:

$$s\begin{bmatrix} x' \\ y' \\ 1 \end{bmatrix} = H\begin{bmatrix} x \\ y \\ 1 \end{bmatrix} \quad (1)$$

where s is the scale factor, H the homography matrix, and (x, y) and (x', y') the coordinates of a set of corresponding points in the two images. The homography transformation aligns any image taken with random camera pose to a reference image, while the scale factor translates pixel coordinates to a metric system, thus allowing to correctly measure any distances along the reference plane defined by the markers. The scale factor is calculated based on the distance of the markers which is predefined by the user.

## 3. Image processing procedure and experiments

The images taken from the test setup are processed to find the position of the marker areas within each photo. The image processing code was developed in the MATLAB environment [42]. The procedure is as follows:

1. The image is turned into a gray-scale photo where the intensity of each pixel is between 0 (black) and 1 (white). An example of such a picture is shown in Fig. 7 in step 1.
2. Because the markers are shining, they present high values of intensity, i.e. values close to 1, in the grayscale picture (see the 2nd step in Fig. 7). In an iterative procedure, several thresholds of intensity values are used ranging from 0.6 to 1.0.
3. In each step of this iteration, pixels below the threshold value are turned into black and the rest into white. A binary (i.e. black and white) image is obtained in this way.
4. In the binary image, boundaries are defined. A boundary is an island of connected white pixels in a black background.
5. A geometric compatibility check is applied on each boundary. According to this, too large or too small boundaries, boundaries that are not square-like, or boundaries that are not towards the middle of the photo are eliminated.
6. If exactly 8 boundaries remained after the geometric compatibility check, and if the distance ratios between these boundaries are similar to those distance ratios of the actual markers, then this iteration with this light intensity factor is flagged as appropriate.
7. Marker positions obtained from an iteration flagged as appropriate, are then used for calculating the geometric error, Δ, as shown in Eq. (4). The light intensity factor, which gives the smallest geometric error (Δ), is accepted as the best iteration, and the rest of the steps are conducted by using this light intensity limit obtained from this iteration. For instance, in the example image of Fig. 7, the value of 0.96 was estimated as the best intensity limit. If the image in the second step of Fig. 7 is vertically cut at 0.96, then the plot in the third step of the same figure is obtained. In the third step, the markers are detected together with other shining surfaces, but the geometric tests eliminate the non-compliant surfaces and filter out the markers only.

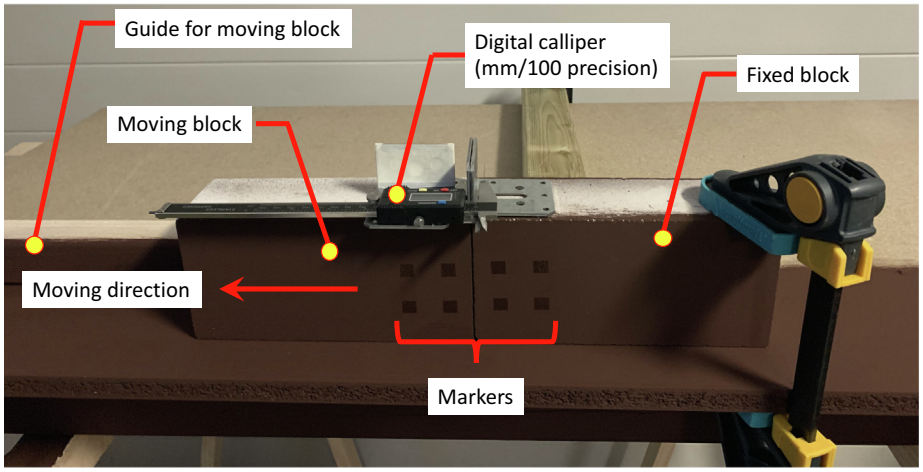


**Fig. 5.** Test setup used in the herein study to evaluate the accuracy of the measurements with the NIR markers.

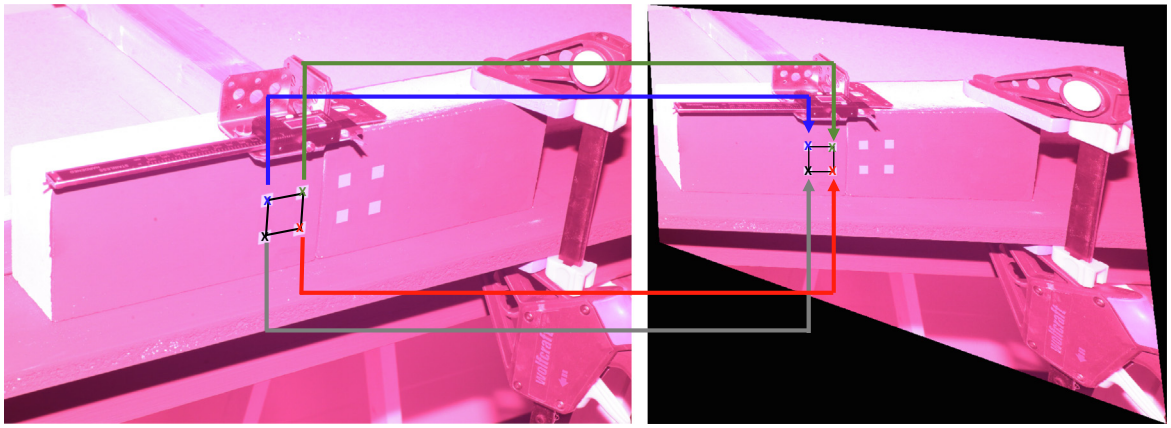


**Fig. 6.** An example of perspective correction with the test setup used in this study.

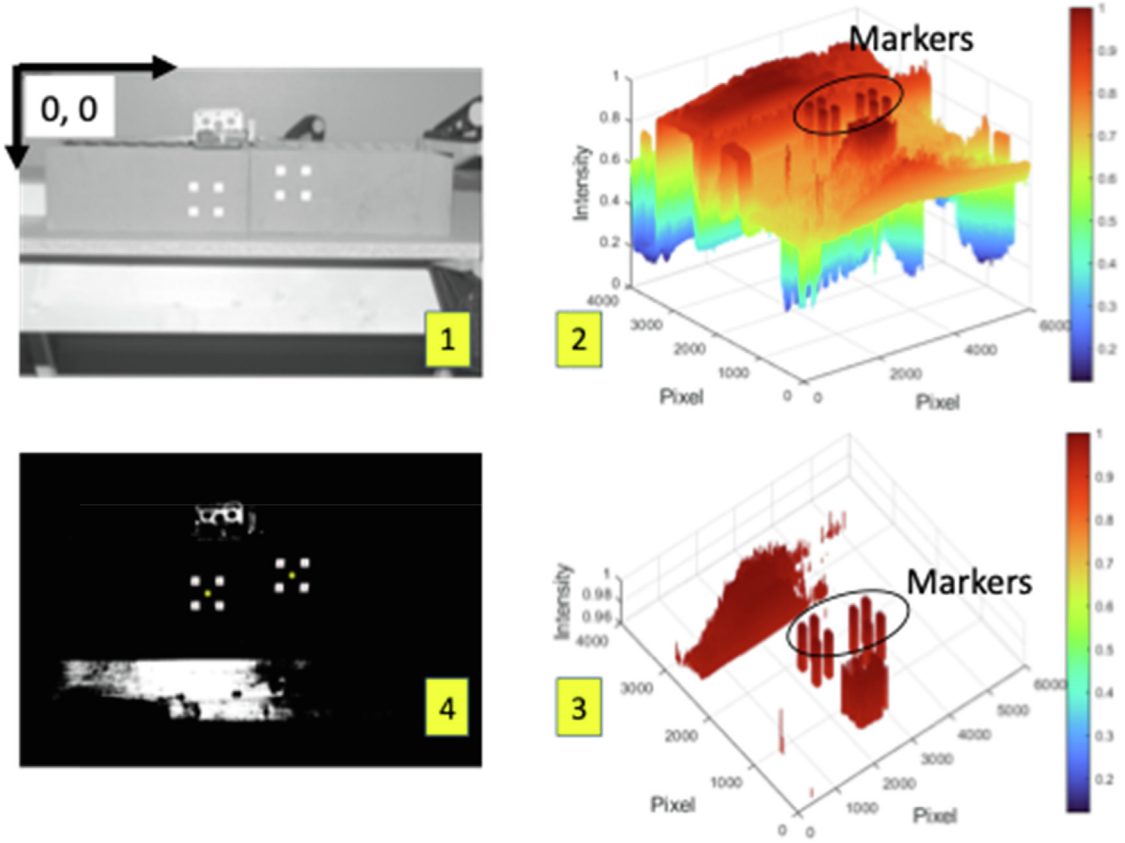


**Fig. 7.** Steps of the image processing; (1) grayscale image, (2) intensity distribution in the grayscale image from 0 to 1, (3) pixels with intensity lower than the threshold value of 0.96 are discarded, (4) binary image created by using 0.96 as intensity threshold, and the markers automatically spotted by using the geometric compatibility checks.

8. Once the best threshold value is determined iteratively, then the marker positions, centroids and quadruple centroids are calculated pixelwise. One of the marker quadruples is used for perspective correction of the image as explained in Section 2.5. The centroids of the four markers in one quadruple are defined as a perfect square and the image is aligned in respect to the reference image forming a perfect square at the location of the quadruple.
9. A new and perspective-corrected image is obtained. Geometric compatibility checks are once more applied on the perspective-corrected image and the new positions and the pixel coordinates of the 8 markers are re-calculated along the reference plane.
10. Pixel coordinates are translated to a metric system. A pixel-to-metric scale factor is calculated based on the distance of the markers, which is predefined by the user. By using this

conversion, actual dimensions and the separation between the marker quadruples are calculated along the plane of the markers.

The geometric error, ($\Delta$) is calculated as:

$$\delta_{left} = \left| \frac{\left(\frac{LM_{52}}{LM_{61}} - \frac{LA_{52}}{LA_{61}}\right)}{(LA_{52}/LA_{61})} \right| \quad (2)$$

$$\delta_{right} = \left| \frac{\left(\frac{LM_{74}}{LM_{83}} - \frac{LA_{74}}{LA_{83}}\right)}{(LA_{74}/LA_{83})} \right| \quad (3)$$

$$\Delta = \frac{(\delta_{left} + \delta_{right})}{2} \quad (4)$$

where $LM_{ij}$ is the pixel-wise distance measured in the image processing algorithm between marker 'i' and marker 'j', $LA_{ij}$ is the actual distance between the same markers of 'i' and 'j'. These distances are measured between the diagonals of each marker quadruple (see Fig. 1(a) for the marker numbering). In an ideal situation, the geometric error ($\Delta$) should equal to zero. The higher values departing from zero translate to higher errors of the measurement.

The results are presented in terms of the agreement of the measured separation with the actual separation of the brick blocks. In order to evaluate the reliability of the measurements two metrics are used, i.e. accuracy and precision, which are calculated as shown below. Accuracy is the correctness of a measurement, while precision shows the statistical dispersion of the results. A higher dispersion means less precise results, in other words, higher measurement-to-measurement variations. The formulae for accuracy and precision are given below in Eq. (5) and Eq. (6) (see Nishiyama et al, 2015 [35] for a similar approach).

$$Accuracy = \sqrt{\frac{\sum (x - x_0)^2}{n}} \quad (5)$$

$$Precision = \sqrt{\frac{\sum \left( x - \frac{\sum_{i=1}^{n} x}{n} \right)^2}{n}} \quad (6)$$

where n the is the number of measurement data, while x and $x_0$ are the measured and actual separations, respectively. Comparison of the measured versus actual separation is satisfactorily good as shown in Fig. 8. It would normally be expected that the closer the camera to the markers the better the measurement would be. This may be correct in normal markers, since a closer photo means a larger number of pixels fitting into a marker boundary, minimizing the pixel-wise errors. Nevertheless, this is not the case in the NIR markers since the photo is illuminated with a strong NIR flash and the reflection amount is dominated by the intensity and the angle of the flashlight on the surface. This issue can be more clearly seen in Fig. 9 where accuracy and precision of measurements are

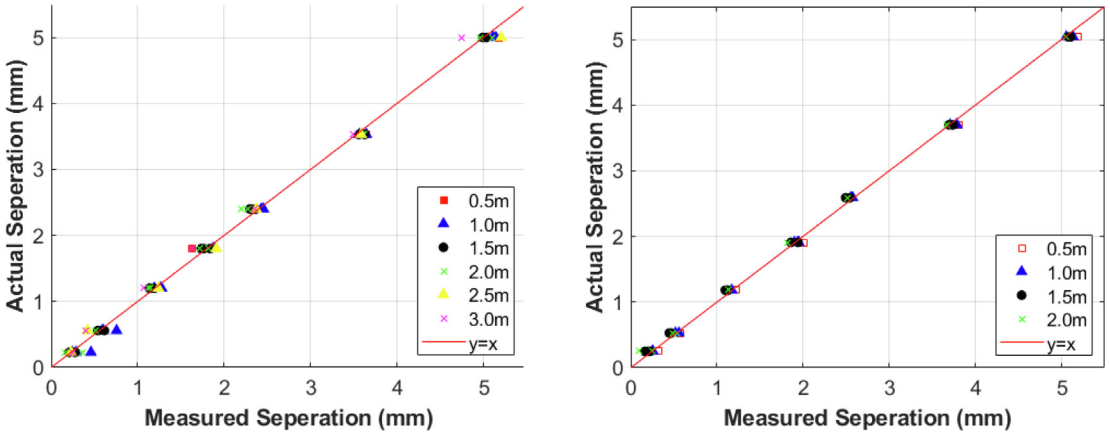


**Fig. 8.** Comparison of the measured vs actual separation of the brick blocks; tape markers (left), and the paint markers (right).

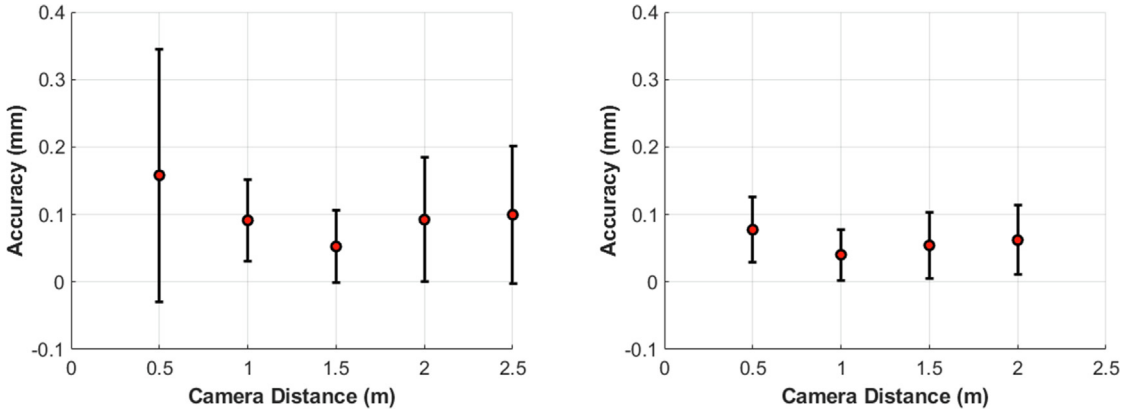


**Fig. 9.** Accuracy of the measurements from multiple photos with a varying range of flash intensities (vertical lines represent the precision of the measurement); tape markers (left), and the paint markers (right).

presented for each distance. The accuracy values are worse for the closest distance (0.5 m) in both marker types. The reason for this is that the strong flash creates a strong reflection on the surfaces of the object, creating a noise around the edges of the markers. These arbitrary edges then shift the centroid of the marker boundaries, leading thus to an error in the measurements. The best picture distance is 1.5 m in the tape markers and 1.0 m in the painted markers, provided that the exposure parameters are used as described above. This is a very practical information since approaching the walls more than 1–1.5 m is most of the times not possible or allowed. It is reminded that for the whole set of experiments the focal length is kept equal to 55 mm in an 18x55 lens, while the larger distances could also work with a lens with a higher zoom capability.

Another observation is that the painted markers perform better than the tape markers both in terms of accuracy and precision. It is possible to obtain 0.05 mm accuracy and 0.04 mm precision with the painted markers. The accuracy and precision can be 0.05 mm and 0.052 mm respectively in the case of tape markers, respectively. Considering that the crack widths start to be noticeable by the human eye from 0.1 mm [43], accuracy and precision of both markers are satisfactory for practical use in masonry brick or plastered and painted masonry surfaces, thus the proposed method can reliably replace crack monitoring sensors.

## 4. Conclusions

Historical buildings with acute structural problems, aging masonry structures and infrastructure inventory (masonry arch bridges, tunnels, viaducts etc.) need increasingly more attention. Higher operational loads, change of their use, extreme loads like induced or natural earthquakes, and strains imposed by the climate change are the major threats to the aging masonry built stock. Failure of such structures and infrastructure could lead to significant direct and indirect costs to the economy and society, and for example could hamper rescue and recovery efforts after a major earthquake. The cost of replacing masonry infrastructure in Europe alone would run into tens of billions of euros. Last but not the least, in most cases the aesthetic and heritage value of masonry infrastructure is also a significantly important parameter.

Visual inspection is a manual process that has been used internationally for keeping track of the health condition of masonry structures and monitoring the progress of damage. However, the manual method is time consuming and subjective (giving rise to variance in standards and quality), which makes the task of prioritising repair, renewal or refurbishment schemes extremely difficult. Human-based inspections are also highly costly and difficult to manage when a large number of structures needs to be assessed.

Alternative technological methods, such as photographic techniques, which are more efficient and reliable, could help meeting the challenges of examining of these structures; especially the identification and monitoring of crack development. Although there are very sensitive Digital Image Correlation (DIC) techniques widely available for the laboratory applications and for experiments, they need surface preparation or require markers that are easily visible, disturbing the aesthetic look of a structure. Furthermore, in such laboratory applications, the camera needs to remain in a fixed position while strong background flash light is also a necessity. When dealing with real structures and particularly with historical buildings, such practices are not possible to be applied, instead, aesthetically acceptable methods with minimum footprint are needed.

In this paper proposed is a technique for measuring cracks in masonry structures using a digital camera. Two different types of markers, which are not easily noticeable by human eye but exhibit high reflection when subjected to NIR (near-infrared) wavelength of light, were used. The first type of marker was a retroreflective one covered by a special tape that is opaque in visible light but translucent in NIR. The second marker was a paint produced from infrared reflective pigments. The markers were placed at brick surfaces and digital camera images of the targets were processed by a custome-madeimage processing algorithm. A series of experiments were conducted to verify the potential of approach as well as the measurement accuracy and precision. Measurements obtained from image processing were compared against the manual measurements. From the results of the processing, it was shown that:

- Separation distance of bricks, representing cracks, was measured by image processing and compared to the actual separations,
- A camera, held in hand and up to 2.5 m distance to the brick surface, was able to capture photographs that provide high accuracy, which was below 0.1 mm in average in most cases,
- The accuracy values were worse for the closest distance (0.5 m) in both marker types, due to the strong flash reflection on the surface,
- The best picture distance is 1.5 m away from the target for the tape markers, and 1.0 m for the painted markers, provided that the proposed camera settings were used,
- The painted markers perform better than the tape markers both in terms of accuracy and precision,
- The variation of the accuracy in the case of tape markers was minimum 0.06 mm and maximum 0.17 mm for 1.5 m and 0.5 m camera distances, respectively,
- The variation of the accuracy in the case of paint markers was much smaller, 0.04 mm at minimum and 0.06 mm at maximum, for 1.0 m and 0.5 m camera distances, respectively, and
- For both painted and tape markers, the accuracy could be in the range of 0.05 mm <0.1 mm (crack widths noticeable by the human eye) which verifies the suitability of the approach to measure cracks in masonry walls or plastered and painted masonry surfaces.

The proposed technique is fast and reliable in measuring changes in the crack width. The method is especially useful for historical buildings, for monitoring progression of damages also in slow acting events such as foundation settlements. The technique could also be used by non-technical people, so citizen involvement is possible in collecting data from the field.

In the future, the effects of angle to the wall on the accuracy of the method will be evaluated. Lenses with higher focal length will be examined in the future to allow for measurement from longer distances. In addition, performing further research by taking measurements on actual sites, with the aim to assess reliability and durability of the markers to weather conditions, are planned.

## 5. Data and resources

The complete photograph dataset used for this study is uploaded on a public research database [44]. The DIC code used for the postprocessing of the photos is uploaded on a public repository and can be found at:https://github.com/ihsanenginbal/Image_processing_code_for_8node_NIR_markers.

## CRediT authorship contribution statement

**İhsan E. Bal:** Conceptualization, Methodology, Software, Project administration, Writing - original draft. **Dimitris Dais:** Methodology, Data curation, Software, Writing - review & editing. **Eleni Smyrou:** Methodology, Supervision, Writing - review & editing,

Project administration. **Vasilis Sarhosis:** Methodology, Validation, Supervision, Writing - review & editing.

## Declaration of Competing Interest

The authors declare that they have no known competing financial interests or personal relationships that could have appeared to influence the work reported in this paper.

## Acknowledgements

The introduced method was developed alongside the project "Seismic Monitoring of Historical Buildings in Groningen" funded by Rijksdienst voor het Cultureel Erfgoed, Grant No.: 126761. The work has been partially funded by RVO RAAK MKB programme, within the project "SafeGO - Seismic Monitoring, Design And Strengthening For thE GrOningen Region", Grant No.: RAAK. MKB09.021.

## References

[1] N. Makoond, L. Pelà, C. Molins, P. Roca, D. Alarcón, Automated data analysis for static structural health monitoring of masonry heritage structures, Structural Control and Health Monitoring. 27 (2020) 1–25, https://doi.org/10.1002/stc.2581.
[2] L.F. Ramos, L. Marques, P.B. Lourenço, G. De Roeck, A. Campos-Costa, J. Roque, Monitoring historical masonry structures with operational modal analysis: Two case studies, Mechanical Systems and Signal Processing. 24 (5) (2010) 1291–1305, https://doi.org/10.1016/j.ymssp.2010.01.011.
[3] A. Kita, N. Cavalagli, M.G. Masciotta, P.B. Lourenço, F. Ubertini, Rapid post-earthquake damage localization and quantification in masonry structures through multidimensional non-linear seismic IDA, Engineering Structures. 219 (2020) 110841, https://doi.org/10.1016/j.engstruct.2020.110841.
[4] R. Ceravolo, A. De Marinis, M.L. Pecorelli, L. Zanotti Fragonara, Monitoring of masonry historical constructions: 10 years of static monitoring of the world's largest oval dome, Structural Control and Health Monitoring. 24 (2017), https://doi.org/10.1002/stc.1988 e1988.
[5] L.M.S. Gonçalves H. Rodrigues F. Gaspar L.M.d.S. Gonçalves H. Rodrigues F. Gaspar Nondestructive Techniques for the Assessment and Preservation of Historic Structures 1 CRC Press
[6] A. Carpinteri, G. Lacidogna, Damage Monitoring of an Historical Masonry Building by the Acoustic Emission Technique, Materials and Structures. 39 (2) (2007) 161–167, https://doi.org/10.1617/s11527-005-9043-2.
[7] E. Verstrynge, K. De Wilder, A. Drougkas, E. Voet, K. Van Balen, M. Wevers, Crack monitoring in historical masonry with distributed strain and acoustic emission sensing techniques, Construction and Building Materials. 162 (2018) 898–907, https://doi.org/10.1016/j.conbuildmat.2018.01.103.
[8] S. Acikgoz, M.J. DeJong, C. Kechavarzi, K. Soga, Dynamic response of a damaged masonry rail viaduct: Measurement and interpretation, Engineering Structures. 168 (2018) 544–558, https://doi.org/10.1016/j.engstruct.2018.04.054.
[9] B. Riveiro, M.J. DeJong, B. Conde, Automated processing of large point clouds for structural health monitoring of masonry arch bridges, Automation in Construction. 72 (2016) 258–268, https://doi.org/10.1016/j.autcon.2016.02.009.
[10] R. Napolitano, B. Glisic, Methodology for diagnosing crack patterns in masonry structures using photogrammetry and distinct element modeling, Engineering Structures. 181 (2019) 519–528, https://doi.org/10.1016/j.engstruct.2018.12.036.
[11] N. Kassotakis, V. Sarhosis, B. Riveiro, B. Conde, A.M. D'Altri, J. Mills, G. Milani, S. de Miranda, G. Castellazzi, Three-dimensional discrete element modelling of rubble masonry structures from dense point clouds, Automation in Construction. 119 (2020) 103365, https://doi.org/10.1016/j.autcon.2020.103365.
[12] A.M. D'Altri, G. Milani, S. de Miranda, G. Castellazzi, V. Sarhosis, Stability analysis of leaning historic masonry structures, Automation in Construction. 92 (2018) 199–213, https://doi.org/10.1016/j.autcon.2018.04.003.
[13] A. Salmanpour, N. Mojsilović, J. Schwartz, Displacement capacity of contemporary unreinforced masonry walls: An experimental study, Engineering Structures. 89 (2015) 1–16, https://doi.org/10.1016/j.engstruct.2015.01.052.
[14] M. Shafiei Dizaji, M. Alipour, D.K. Harris, Leveraging Full-Field Measurement from 3D Digital Image Correlation for Structural Identification, Experimental Mechanics. 58 (7) (2018) 1049–1066, https://doi.org/10.1007/s11340-018-0401-8.
[15] P.A. Korswagen, M. Longo, J.G. Rots, High-resolution monitoring of the initial development of cracks in experimental masonry shear walls and their reproduction in finite element models, Engineering Structures. 211 (2020) 110365, https://doi.org/10.1016/j.engstruct.2020.110365.
[16] I.E. Senaldi, G. Guerrini, P. Comini, F. Graziotti, A. Penna, K. Beyer, G. Magenes, Experimental seismic performance of a half-scale stone masonry building aggregate, Bulletin of Earthquake Engineering. 18 (2) (2020) 609–643, https://doi.org/10.1007/s10518-019-00631-2.
[17] S. Kallioras, G. Guerrini, U. Tomassetti, B. Marchesi, A. Penna, F. Graziotti, G. Magenes, Experimental seismic performance of a full-scale unreinforced clay-masonry building with flexible timber diaphragms, Engineering Structures. 161 (2018) 231–249, https://doi.org/10.1016/j.engstruct.2018.02.016.
[18] B.F. Spencer, V. Hoskere, Y. Narazaki, Advances in Computer Vision-Based Civil Infrastructure Inspection and Monitoring, Engineering. 5 (2) (2019) 199–222, https://doi.org/10.1016/j.eng.2018.11.030.
[19] V. Hoskere, Y. Narazaki, T.A. Hoang, B.F. Spencer, MaDnet: multi-task semantic segmentation of multiple types of structural materials and damage in images of civil infrastructure, Journal of Civil Structural Health Monitoring. 10 (5) (2020) 757–773, https://doi.org/10.1007/s13349-020-00409-0.
[20] D. Kang, S.S. Benipal, D.L. Gopal, Y.-J. Cha, Hybrid pixel-level concrete crack segmentation and quantification across complex backgrounds using deep learning, Automation in Construction. 118 (2020) 103291, https://doi.org/10.1016/j.autcon.2020.103291.
[21] Y.J. Cha, W. Choi, G. Suh, S. Mahmoudkhani, O. Büyüköztürk, Autonomous Structural Visual Inspection Using Region-Based Deep Learning for Detecting Multiple Damage Types, Computer-Aided Civil and Infrastructure Engineering. 33 (2018) 731–747, https://doi.org/10.1111/mice.12334.
[22] A. Ji, X. Xue, Y. Wang, X. Luo, W. Xue, An integrated approach to automatic pixel-level crack detection and quantification of asphalt pavement, Automation in Construction. 114 (2020) 103176, https://doi.org/10.1016/j.autcon.2020.103176.
[23] G. Stockdale, V: Sarhosis, G. Milani, Increase in seismic resistance for a dry joint masonry arch subjected to hinge control, 10th IMC Conference Proceedings, (2018) 968-981, International Masonry Society.
[24] G. Stockdale G. Milani V. Sarhosis Increase in seismic resistance for a full-scale dry stack masonry arch subjected to hinge control Key Enginering Materials 817 817KEM(2019) 221 228
[25] G.L. Stockdale, V. Sarhosis, G. Milani, Seismic capacity and multi-mechanism analysis for dry-stack masonry arches subjected to hinge control, Bulletin of Earthquake Engineering 18 (2) (2020) 673–724.
[26] D. Dais İ.E. Bal E. Smyrou V. Sarhosis Automatic Crack Classification and Segmentation on Masonry Surfaces Using Convolutional Neural Networks and Transfer Learning 125 2021 103606 10.1016/j.autcon.2021.103606
[27] A. Rezaie, R. Achanta, M. Godio, K. Beyer, Comparison of crack segmentation using digital image correlation measurements and deep learning, Construction and Building Materials. 261 (2020) 120474, https://doi.org/10.1016/j.conbuildmat.2020.120474.
[28] İ.E. Bal, D. Dais, E. Smyrou, V. Sarhosis, Monitoring of a Historical Masonry Structure in Case of Induced Seismicity, International Journal of, Architectural Heritage. 15 (1) (2021) 187–204, https://doi.org/10.1080/15583058.2020.1719230.
[29] J. Carrillo, D. Dominguez, N. Prado, Seismic Damage Index Based on Fractal Dimension of Cracking on Thin Reinforced Concrete Walls, ACI Structural Journal. 114 (2017), https://doi.org/10.14359/51700919.
[30] A. Farhidzadeh, E. Dehghan-Niri, A. Moustafa, S. Salamone, A. Whittaker, Damage Assessment of Reinforced Concrete Structures Using Fractal Analysis of Residual Crack Patterns, Experimental Mechanics. 53 (9) (2013) 1607–1619, https://doi.org/10.1007/s11340-013-9769-7.
[31] V. Sarhosis, D. Dais, E. Smyrou, İ.E. Bal, Evaluation of modelling strategies for estimating cumulative damage on Groningen masonry buildings due to recursive induced earthquakes, Bulletin of Earthquake Engineering. 17 (8) (2019) 4689–4710, https://doi.org/10.1007/s10518-018-00549-1.
[32] H. Cho, H.-J. Yoon, J.-Y. Jung, Effects of the Ground Resolution and Thresholding on Crack Width Measurements, Sensors. 18 (2018) 2644, https://doi.org/10.3390/s18082644.
[33] X. Yang, H. Li, Y. Yu, X. Luo, T. Huang, X.u. Yang, Automatic Pixel-Level Crack Detection and Measurement Using Fully Convolutional Network, Computer-Aided Civil and Infrastructure Engineering. 33 (12) (2018) 1090–1109, https://doi.org/10.1111/mice:2018.33.issue-1210.1111/mice:12412.
[34] A.E. Wojnarowski A.B. Leonteva S.V. Tyurin S.G. Tikhonov O.V. Artemeva A.E. Wojnarowski, A.B. Leonteva, S. V Tyurin, S.G. Tikhonov, O. V Artemeva, Photogrammetric Technology for Remote High-Precision 3d Monitoring of Cracks and Deformation Joints of Buildings and Constructions, ISPRS–International Archives of the Photogrammetry, Remote Sensing and Spatial Information Sciences. XLII-5/W2 (2019) 95–101. doi:10.5194/isprs-archives-XLII-5-W2-95-2019.
[35] S. Nishiyama, N. Minakata, T. Kikuchi, T. Yano, Improved digital photogrammetry technique for crack monitoring, Advanced Engineering Informatics. 29 (4) (2015) 851–858, https://doi.org/10.1016/j.aei.2015.05.005.
[36] D. Germanese, G. Leone, D. Moroni, M. Pascali, M. Tampucci, Long-Term Monitoring of Crack Patterns in Historic Structures Using UAVs and Planar Markers: A Preliminary Study, Journal of Imaging. 4 (2018) 99, https://doi.org/10.3390/jimaging4080099.
[37] C. Alessandri, Garutti M., Mallardo V., Milani G., Crack patterns induced by foundation settlements: Integrated analyses on a Renaissance masonry Palace in Italy, International Journal of Architectural Heritage, 9(2015) 111-129, doi: 10.1080/15583058.2014.951795.
[38] A. Tralli, A. Chiozzi, N. Grillanda, G. Milani, Masonry structures in the presence of foundation settlements and unilateral contact problems, International

Journal of Solids and Structures 191–192 (2020) 187–201, https://doi.org/10.1016/j.ijsolstr.2019.12.005.
[39] S. Tiberti, N. Grillanda, V. Mallardo, G. Milani, A Genetic Algorithm adaptive homogeneous approach for evaluating settlement-induced cracks in masonry walls, Engineering Structures. 221 (2020) #111073, https://doi.org/10.1016/j.engstruct.2020.111073.
[40] R. Hartley, A. Zisserman, Multiple View Geometry in Computer Vision, Cambridge University Press (2004), https://doi.org/10.1017/CBO9780511811685.
[41] R. Szeliski, Computer Vision, Springer, London, London (2011), https://doi.org/10.1007/978-1-84882-935-0.
[42] MATLAB, Natick, Massachusetts: The MathWorks Inc. (2019). www.mathworks.com.
[43] J.B. Burland, C.P. Wroth, Settlement of Buildings and Associated Damage, in: British Geotechnical Society's Conference on the Settlement of Structures, Cambridge, UK, 1974: pp. 611–654.
[44] I. E. Bal, D. Dais, E. Smyrou, V. Sarhosis, Photos of 8-node NIR markers on masonry bricks, Mendeley Data, v1, 2021. doi: 10.17632/r6g53gtn8m.1.